Journal of Alloys and Compounds 959 (2023) 170259

Contents lists available at ScienceDirect

Journal of Alloys and Compounds

journal homepage: www.elsevier.com/locate/jalcom

Research article

Conventional *s*-wave superconductivity in the non-centrosymmetric compounds Re_3W, $Re_3W_{0.5}Nb_{0.5}$, and $Re_3W_{0.5}Ta_{0.5}$

F. Abud [a,b,*], N. Chaia [c], M.S. Torikachvili [d], R.F. Jardim [a]

[a] Instituto de Física, Universidade de São Paulo, Rua do Matão 1371, 05508–090 São Paulo, SP, Brazil
[b] Escola de Engenharia de Lorena, Departamento de Engenharia de Materiais, Universidade de São Paulo, Lorena, SP, Brazil
[c] Instituto de Ciência e Tecnologia, Universidade Federal de Alfenas, Poços de Caldas, MG, Brazil
[d] Department of Physics, San Diego State University, San Diego, CA 92182, USA

ARTICLE INFO

Article history:
Received 14 February 2023
Received in revised form 11 April 2023
Accepted 22 April 2023
Available online 26 April 2023

Keywords:
Noncentrosymmetric superconductors
Rhenium
Alloying
Pairing mechanism
s-wave superconductivity

ABSTRACT

We carried out an investigation of the structural and superconducting properties of $Re_3W_{1-x}M_x$ alloys, which can crystallize in both a centrosymmetric (CS) hexagonal, and a non-centrosymmetric (NCS) cubic α-Mn phase. The superconducting transition temperatures (T_c) of the CS and NCS phases in pure Re_3W are ~ 9.1 and ~ 7.7 K, respectively. While boules fast cooled from the melt have a mixture of CS phases, the NCS phase can be stabilized upon annealing at very high temperatures (~ 1700 °C), or upon the partial substitution of the transition metals M = Ta, or Nb for W. X-ray diffraction and wavelength dispersive X-ray spectroscopy (WDS) data suggest that the optimal composition for the formation of the α-Mn phase directly from the melt in $Re_3W_{1-x}M_x$ is $x \approx 0.5$. A detailed study of the superconducting properties of the $Re_3W_{1-x}M_x$ solid solutions was carried out by means of measurement of magnetization, *ac* magnetic susceptibility, electrical transport, and low temperature specific heat. As the M content is increased, the superconducting critical temperature T_c progressively decreases, though the overall superconducting properties remain similar to those of the parent NCS Re_3W compound. The partial substitution at the W site does not seem to affect the pairing mechanism. Given the exponentially vanishing character of the electronic specific heat C_e (T) at low temperatures, the superconducting behavior of the NCS alloys is consistent with a nodeless, *s*-wave superconducting gap symmetry in all NCS samples. These findings add the pseudo-binary Re-M-W systems to the small roll of NCS materials where the pairing symmetry of the superconducting state can be explored.

1. Introduction

While global gauge symmetry is a key element of the superconducting state, parity is the key symmetry regarding non-centrosymmetric (NCS) superconductors. The absence of an inversion center in the crystal structure of NCS materials breaks the parity symmetry and leads to anti-symmetric spin-orbit coupling (ASOC), therefore lifting the twofold spin degeneracy of conduction band electrons [1]. Cooper pairs without a unique spin component can then be formed on the spin-split bands. Therefore, coexistence of spin singlet and triplet superconducting states is no longer prohibited by symmetry constraints [2,3].

Among the weakly correlated class of materials, the family of Rhenium-based NCS materials has recently drawn attention due to the simultaneous occurrence of time-reversal symmetry breaking (TRSB) in the superconducting state and conventional *s*-wave superconducting order parameter. These apparently opposing features have been proposed to occur in Re_6M (M = Hf, Zr, Ti) [4–7] and $Re_{0.82}Nb_{0.18}$ [8]. On the other hand, zero-field muon-spin-rotation (μSR) data suggest that the time-reversal symmetry remains preserved in Re_3W, Re_3Ta, and $Re_{5.5}Ta$ [9–11] even though all the materials share the same α-Mn NCS crystal structure. To further complicate the experimental picture, the elemental centrosymmetric (CS) Re, having a superconducting critical temperature T_c ~ 2.7 K, exhibits a small internal magnetic field in the superconducting state [8], seemingly ruling out the NCS crystal structure as the origin of the TRSB in Re-based superconductors.

Given the complex phase diagram of the binary Re-W alloys, and melting temperatures exceeding 2000 °C [12], it is difficult to synthesize single-phase Re-W compounds. This is particularly true for

* Corresponding author at: Instituto de Física, Universidade de São Paulo, Rua do Matão 1371, 05508–090 São Paulo, SP, Brazil.
E-mail address: fabio.abud@usp.br (F. Abud).

https://doi.org/10.1016/j.jallcom.2023.170259
0925-8388/

the NCS phase, which lies close to the Re:W ratio of 3:1. Depending on the synthesis route for producing polycrystalline samples, two polymorphs are known to form with the Re_3W composition: one possessing a CS structure and the other with the NCS form. As-cast, arc-melted samples of Re_3W crystallize mostly in the CS structure, previously associated with the hexagonal pure rhenium structure (space group $P6_3/mmc$ - Re-h.c.p. type). This CS phase can be transformed into the NCS cubic phase (space group $I\bar{4}3m$ - α-Mn-type) upon annealing at temperatures exceeding 1500 °C under very low O_2 pressure. The CS phase can be reversed back by arc melting [13]. The CS and NCS phases have distinct T_c's of ~ 9.4 and 7.8 K, respectively.

In this work we probe the effect of the partial substitution of Nb and Ta for W on both the phase formation and the superconducting properties of the $Re_3W_{1-x}(Nb, Ta)_x$ for x = 0 and 0.5. Although the Re-Ta-W ternary phase diagrams reveals the occurrence of the NCS α-Mn phase [14], the superconducting properties of these phases remained largely untested. As it turns out, the partial substitution of the lighter Nb or Ta for W promotes the formation of the α-Mn phase *in as-cast materials*, the samples are superconducting, and the ASOC is considerably weakened. Given the improved phase stability and weakened ASOC strength, a detailed study of the potential crossover from conventional to unconventional superconductivity is in order. The superconducting behavior of the NCS $Re_3W_{1-x}(Nb,Ta)_x$ solid solutions seems consistent with the conventional *s*-wave BCS framework, with no experimental evidence for triplet pairing.

2. Experimental details

Polycrystalline samples of Re_3W, $Re_3W_{0.5}Nb_{0.5}$, and $Re_3W_{0.5}Ta_{0.5}$ were synthesized by arc melting in a home built apparatus. Stoichiometric amounts of high purity Re (99.95 %), W (99.9 %, Nb (99.99 %), and Ta (99.99 %) from Alfa Aesar were placed on top of a water-cooled copper hearth, and arc melted together in a Ti-gettered ultra high purity Ar atmosphere, using a tunsten tip. The boules were turned over and melted again at least four more times in order to ensure homogeneity. The weight loss was lower than 0.5 % and it was not compensated by the addition of the constituents. The resulting samples, hereafter referred to as "as-cast" (AC), were then cut in half; one half remained AC while the other, hereafter referred to as AN, was wrapped in Ta foil, annealed in high vacuum (~ 10^{-6} atm) at 1700 °C for 10–30 h, and cooled rapidly.

X-ray diffraction (XRD) measurements at room temperature were conducted on powdered and bulk samples using a Bruker D8 Advance diffractometer in Bragg-Brentano geometry equipped with Cu-$K_{\alpha 1}$-radiation (λ = 1.5406 Å). The microstructure of the $ReW_{1-x}(Nb, Ta)_x$ samples was examined with a TESCAN MIRA-3 and a Zeiss LEO Stereoscan S440 operating in the backscattered electron (BSE) imaging mode. The chemical composition of the samples was determined by wavelength dispersive X-ray spectrometer (WDS) (from INCA/Oxford).

Magnetization and *ac* magnetic susceptibility data were obtained with a Quantum Design SQUID magnetometer (MPMS), and the ACMS II option for the Physical Property Measurement System Dynacool (PPMS). The temperature dependent magnetization data M (T) were acquired in field-cooled (FC) and zero-field cooled (ZFC) modes. For the ZFC measurements the sample was first cooled down to 2 K in zero field, a small field was applied (typically H = 5 Oe), and magnetization data was collected upon warming. The *ac* measurements were conducted using a drive frequency of 155 Hz and an amplitude of 1 Oe, while the dc external field was maintained at H = 5 Oe. Heat capacity and electrical resistivity measurements were carried out using the dedicated options of the PPMS, relying on a relaxation method and four-lead methodology, respectively. For the electrical resistivity measurements, four gold leads were attached to parallelepiped-shaped samples using Ag paint. The typical dimensions of the samples were ~ 2 × 1 × 0.2 mm³ .

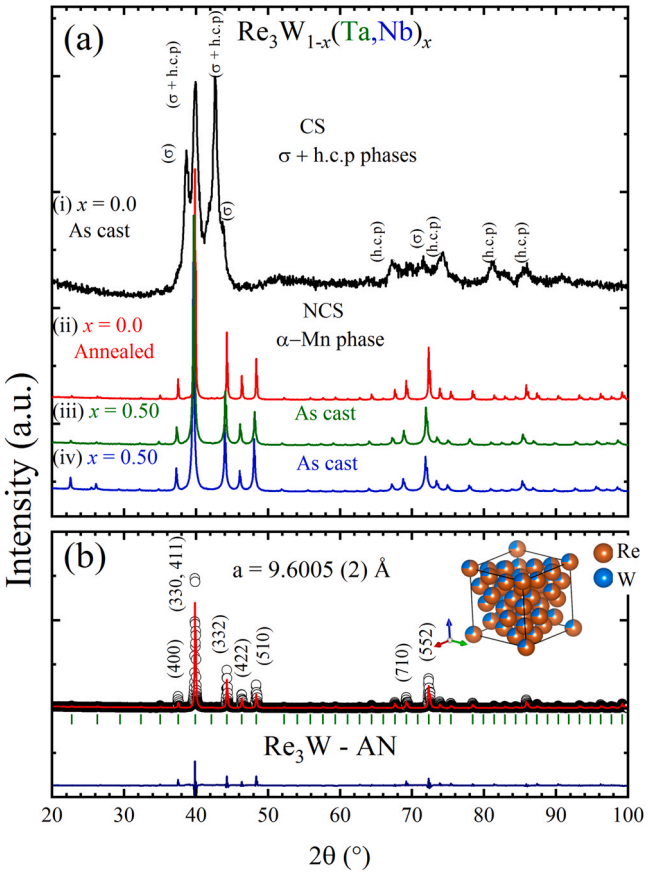

Fig. 1. (a) X-ray diagrams of AC (i) and AN (ii) Re_3W and the AC $Re_3W_{0.5}Ta_{0.5}$ (iii) and $Re_3W_{0.5}Nb_{0.5}$ (iv) solid solutions. The data is offset for clarity. The AC Re_3W diagram (black line on top) exhibit features of a multi-phase (σ + Re-h.c.p.) material, being markedly distinct from the single-phase (α-Mn) diagrams. (b) Rietveld refinement of the AN Re_3W data confirming the single-phase character of the material, as is also the case of both AC alloys $Re_3W_{0.5}Ta_{0.5}$ and $Re_3W_{0.5}Nb_{0.5}$ shown in (a).

3. Experimental results

Except for the AC Re_3W sample, all as-cast specimens were brittle and easy to grind, yielding fine powders appropriate for structural studies by means of X-ray powder diffraction (XRD). However, the parent compound Re_3W could only be ground after annealing at 1700 °C under high vacuum, reflecting a full transformation to the α–Mn phase. Shown in Fig. 1 are the powder XRD diffractograms for the AC and AN $ReW_{1-x}(Nb, Ta)_x$ samples with x = 0 and 0.5. The scan of Fig. 1(a)(i) was taken on a polished flat surface of the AC Re_3W material, and a careful analysis of the XRD data indicates the presence of at least two phases, including the CS σ phase and hexagonal phases. The σ phase is tetragonal (space group $P4_2/mnm$), whose prototype material is CrFe, and it is closely related to the α–Mn (or also known as χ) phase, and both can be included in the Frank-Kasper family of topological phases [15,16]. The σ phase is considered to be the most stable phase within the Re-W alloys with Re contents lower than 75 at%. The presence of the σ phase in AC Re_3W, which we report here for the first time, was not identified in previous studies [13,17].

The exact atomic composition of the AC Re_3W sample could not be unambiguously determined from the XRD data alone, primarily due to the large width of the most intense reflections. However, the coexistence of the σ and Re-h.c.p. phases in the AC Re_3W specimen is

conceivable, given the well-known progression of the structure from single Re-h.c.p. in $Re_{0.9}W_{0.1}$ to single-phase σ in $Re_{0.5}W_{0.5}$ (see Fig. S1 in Supplementary material), as well as for the microstructural details of the AC Re_3W material, which we'll discuss later. Therefore, the main reflections of the XRD scan in Fig. 1(a)(i) are indexed in analogy to the Bragg reflections observed in as-cast $Re_{0.82}W_{0.18}$, $Re_{0.67}W_{0.33}$, and Re_3W specimens. Given the large width of the reflections, it is not possible to completely rule out the nucleation of a small amount of the NCS α–Mn as a minority phase. In contrast, the XRD data for the well established two-phase Re-W materials, having the α–Mn as a minor phase (shown in Supplementary material, section S2), yield radically different scans from the ones shown in Fig. 1(a)(i).

The powder XRD scan for the Re_3W sample annealed at 1700 °C is shown in Fig. 1(a)(ii), and it displays only reflections belonging to the NCS α-Mn type structure. This transformation from the CS phase to a purely α-Mn phase is consistent with the peritectoid transformation (Re-h.c.p. + σ → α-Mn) taking place upon annealing at 1700 °C [12]. This transformation to a single-phase is reminiscent of the Re-Mo system [18], where single-phase α-Mn materials have only been obtained upon annealing at high temperatures. The lattice parameters of the single-phase samples were then calculated from Rietveld refinements using the Fullprof suite [19]. The refined XRD diagram for the α-Mn phase Re_3W is displayed in Fig. 1(b), and the calculated lattice parameters for all samples are listed in Table 1. The calculated lattice parameter of the AN Re_3W was found to be a = 9.6005(2) Å, showing good agreement with the range 9.5965–9.599 Å reported in neutron diffraction studies [13,20]. According to Fig. 1(a), the Bragg peaks of the solid solution samples are shifted to lower angles in relation to those of the pristine AN Re_3W, clearly indicating an enlargement of the lattice parameter upon the partial atomic substitution. Therefore, this enlargement is confirmed by the Rietveld refinements, which yielded a = 9.642 and 9.647 Å for the $Re_3W_{0.5}Ta_{0.5}$ and $Re_3W_{0.5}Nb_{0.5}$ AC materials, respectively. Although larger than that of the Re_3W parent compound, the lattice parameters of the solid solutions are smaller than those of Re_3Ta (9.691 Å) and Re_3Nb (9.689 Å); those values were obtained in our samples and are in agreement with the reported ones [10,21,22]. As expected for a solid solution system, we have confirmed that the lattice parameters of the $Re_3W_{1-x}(Ta,Nb)_x$ materials grow monotonically with the substitution level x, closely following the Vergard's law ($a_{Re3W1-x(Nb,Ta)x} \sim (1\text{-}x)\ a_{Re3W} + x\ a_{Re3(Nb,Ta)}$).

In contrast to Re_3W, AC Re_3Ta and Re_3Nb both crystallize in the α-Mn structure right from the melt (see Supplementary material, section S3), although annealing at high temperatures improves slightly the phase purity and homogeneity. It is thus tempting to consider that the partial substitution of Ta or Nb for W in Re_3W facilitates the formation of the α-Mn phase upon casting. We found that the 50 % substituted $Re_3W_{0.5}Ta_{0.5}$ and $Re_3W_{0.5}Nb_{0.5}$ solid solutions solidified from the melt with the α-Mn structure, as indicated by the XRD scans of Fig. 1(a) (iii and iv). Therefore, the partial atomic substitutions promote the α-Mn phase stability, in addition to widening the solubility limit of the α-Mn phase, according to the ternary phase diagram above 1500 °C proposed for Re-Ta-W [14].

Table 1
Superconducting and normal state parameters of the annealed $Re_3W_{1-x}M_x$; M = Nb, Ta; x = 0, 0.5, and 1.

	Re_3W	$Re_3W_{0.5}Ta_{0.5}$	Re_3Ta	$Re_3W_{0.5}Nb_{0.5}$	Re_3Nb
T_c (K)	7.7	6.9	4.75	7.6	6.3
RRR	1.15	1.12	1.04	1.12	1.05
ρ (μΩcm)	171	231	280	252	307
a (Å)	9.601	9.642	9.691	9.647	9.689
γ_n (mJ mol^{-1} K^{-2})	17.1	17.4	13.3	17.9	16.3
Δ_0 (meV)	1.29	1.14	-	1.28	-
$2\Delta_0/k_BT_c$	3.86	3.85	-	3.91	-
$\Delta C_p/\gamma_nT_c$	1.58	1.61	1.57	1.71	1.48

In order to further probe the effect of the substitutions on the formation of the α-Mn phase, one can rely on the information from the binary phase diagrams of the Re-Ta and Re-W systems (Figs. 2(a) and 2(b), respectively). The single-phase α-Mn field (yellow highlight) is quite different in the two systems, as far as the solidification temperatures and solubility range. The transformation of two solid phases (Re-h.c.p. and σ) is required to stabilize the α-Mn phase in the Re-W system (peritectoid reaction), in contrast to the congruent melting transformation observed in the Re-Ta system, that leads the liquid phase directly into the α-Mn solid phase. In the latter case, the small temperature gap between the solidus and liquidus lines along the broad α-Mn solubility range is responsible for the straightforward formation of single-phase Re_3Ta directly from the melt (i.e. as-cast), without phase segregation. Similar phase formation behavior is observed in the Re-Nb system (data not shown).

The details of the Re-W, Re-Ta, and Re-Nb binary systems suggest that the partial substitution of Ta or Nb for W alters the α-Mn single-phase field, transitioning it to an intermediary format in the ternary Re-Ta-W system, i.e. the partial substitutions both widens the solubility limit and drives the peritectoid Re-W temperature towards the liquidus line. The substitution level eventually reaches the values where the pseudo-binary material melts congruently. Therefore, the phase segregation upon solidification in the Re-W system can be avoided with partial substitutions. As shown in the Supplementary material, phase segregation remains present in as-cast $Re_3W_{1-x}(Ta,Nb)_x$ at minor substitution levels ($x \approx 0.1$) in $Re_3W_{0.9}Ta_{0.1}$ and $Re_3W_{0.9}Nb_{0.1}$. Atomic substitutions $x \approx 0.25$ changes the overall phase composition drastically, yielding as-cast materials nearly single-phase, with just one unidentified reflection with very low intensity at $2\theta \sim 42.7°$ in $Re_3W_{0.75}Ta_{0.25}$. A further increase in substitution level to $x \approx 0.5$ yields single-phase as-cast materials, as displayed in Fig. 2(d).

In order to illustrate the effect of the partial substitutions on phase formation, the 1500 °C isothermal section of the Re-Ta-W system is displayed in Fig. 2(c). Although this isothermal section is quite far in temperature from the liquidus-solid boundary line near the 75%at. Re content, the diagram is helpful, as it shows the continuous broadening of the α-Mn phase field, as the substitution level ***x*** is increased in the $Re_3W_{1-x}Ta_x$ series. This broadening is consistent with the ability of the α-Mn structure to accommodate the off-stoichiometry compositions by means of substitutions at the four sites of the structure [26]. This ability is somewhat limited in the Re-W binary system, but it is largely enhanced as the Ta or Nb content is progressively increased. Therefore, the atomic substitutions of Ta or Nb for W are also consistent with the increase of site disorder, which is already present in annealed Re_3W.

The ternary phase diagram Re-Ta-W (Fig. 2(c)) suggests that the solid solutions can be homogenized in heat treatment at 1500 °C under very high vacuum. Thus, heat treatments at temperatures above 1500 °C (~ 1700 °C in the case of this work) significantly decrease the time required to attain optimally homogenized materials. An expanded view of the Re-rich region is shown in Fig. 2(d). The $Re_3W_{0.5}Ta_{0.5}$ is deep inside the single-phase field, suggesting that heat treatments in temperatures above 1500 °C avoid the precipitation of other phases, while possibly further promoting the homogeneity of the α-Mn phase.

A SEM study of the microstructure supports the phase composition findings of the XRD data and phase diagram analysis, i.e. the α-Mn phase formation in the Re-W system obtained by heat treatment and the promotion of this phase by partial substitutions. Shown in Figs. 3(a) and 3(b) are SEM/BSE images of the AC Re_3W sample. The microstructure shows the Re-h.c.p. and σ phases, in good agreement with the Re-W phase diagram, whose region close to 75%at. Re is depicted in Fig. 2, and the XRD measurements. The subtle contrast seen in the micrographs is due to regions with slightly different mean atomic number, ranging from 74.8 to 74.9 in the $Re_{0.82}W_{0.18}$

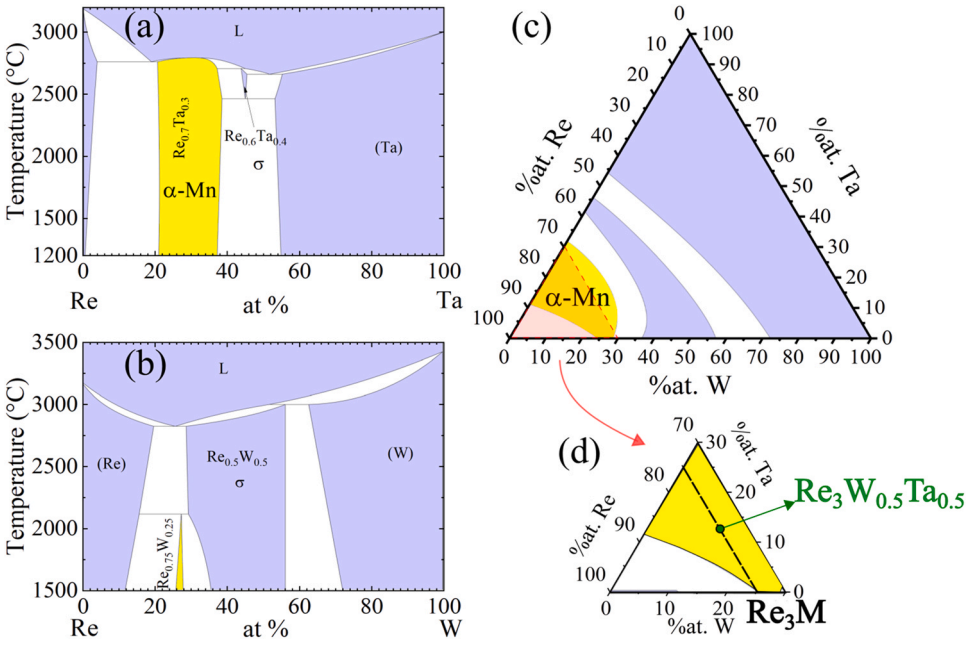

Fig. 2. Equilibrium phase diagrams of the Re-Ta (a) and Re-W (b) systems are displayed in the left side of the figure. Panel (c) exhibits the isothermal section at T = 1500 °C of the ternary Re-Ta-W system. An expanded view of the rhenium-rich portion of the ternary diagram is depicted in (d). The single-phase NCS α-Mn fields are highlighted in yellow in all the diagrams. Binary phase diagrams Re-Ta, Re-W, and the ternary Re-Ta-W were adapted from Refs. [23,24], and [25], respectively.

(Re-h.c.p.) and $Re_{0.66}W_{0.33}$ (σ) compositions, respectively. An elemental quantitative analysis using WDS was carried out at the 9 locations along the ~ 100 μm line shown in Fig. 3(b), and the relative concentrations of Re and W are shown in Fig. 3(d). These data show a high level of inhomogeneity, and a rather large fluctuation in the chemical composition throughout the material, with substantial deviations from the 75 % at. Re nominal value (dashed lines). Two compositions are confirmed: one with approximately 80 % at. Re, indicated by the blue points in Fig. 3(d), due to the presence of the Re-h.c.p. phase, and the other with Re content below 70 % at., in red, most likely associated with the σ-phase. These data also suggest that given the rapid cooling of the AC materials, the solid solution (Re-h.c.p./σ) maybe retained upon freezing, since this phase lies above the peritectic temperature, as illustrated in Fig. 3(c), resulting in a dendrite-like microstructure.

Shown in Fig. 4(a) and Fig. 5(a) are the micrographs for the AN Re_3W and AC $Re_3W_{0.5}Ta_{0.5}$ specimens, respectively. The BSE image for AN Re_3W (Fig. 4(a)) is clearly different from its AC counterpart (see Figs. 3(a) and 3(b)), as the α-Mn phase stabilization is reflected in the more homogeneous image. Although being more uniform, the AN micrographs exhibit a few darker regions, suggesting that a very low volumetric fraction of micro segregations still remains present after the 1700 °C heat treatment in high vacuum. The WDS analysis displayed in Fig. 4(b) shows that the expected atomic ratio Re:W of 75:25 (dashed lines) is approximately met in the main portion of the material while it becomes Re-rich (80:20) only in the selected points

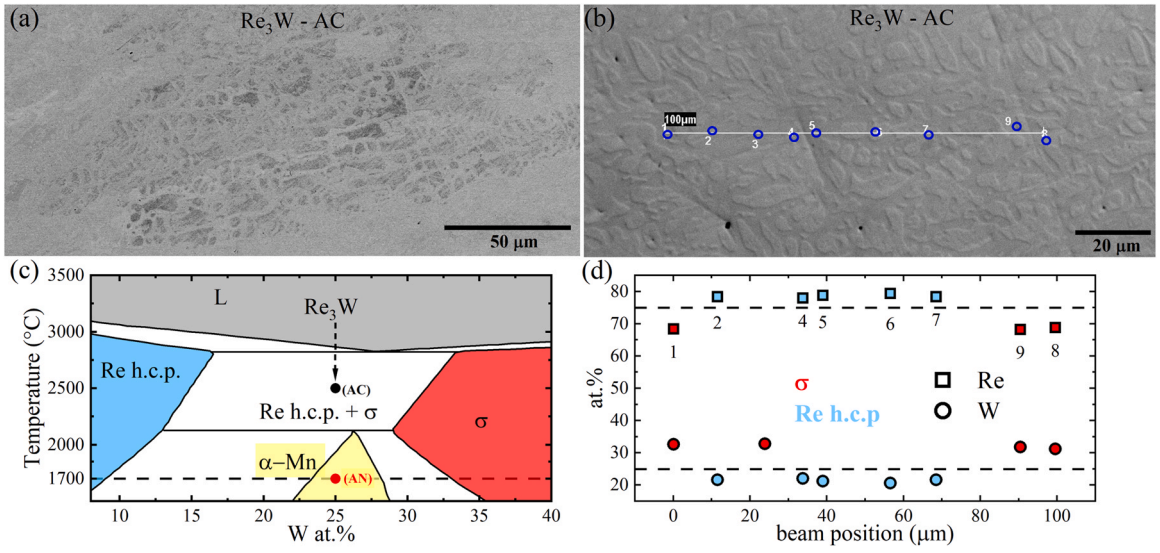

Fig. 3. (a) and (b) SEM/BSE images for distinct segments of the AC Re_3W alloy. The blue highlighted points in (b) are the positions where WDS microanalyses were conducted. (c) Expanded view of the Re-W phase diagram, focusing on the high temperature, rhenium-rich side. The black dashed arrow illustrates the cooling process in AC materials. (d) Concentration profile measured with WDS at the enumerated points in (b): the horizontal dashed lines represent the nominal composition (in at%) of the AC Re_3W specimen. The rhenium deficient red data points are related to the σ phase while the blue ones are associated to the Re-rich h.c.p. phase.

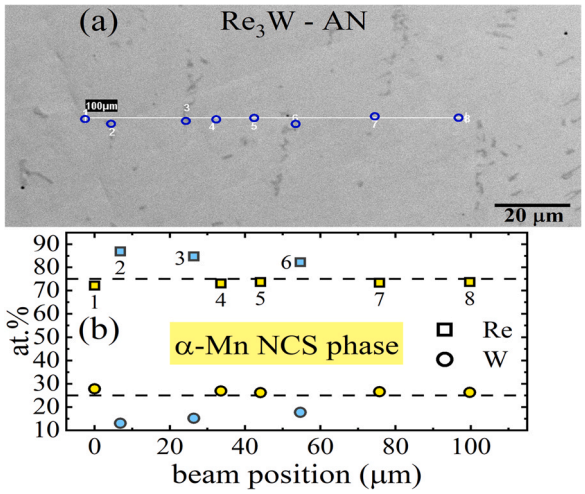

Fig. 4. (a) SEM/BSE images of the AN Re_3W alloy; (b) Concentration profile measure at the enumerated, blue highlighted points in the micrograph (a). The yellow data points represent the regions where the Re:W atomic ratio is approximately 3:1 (brighter regions in the micrograph), and the data in blue are related to Re-rich micro-segregations (darker areas).

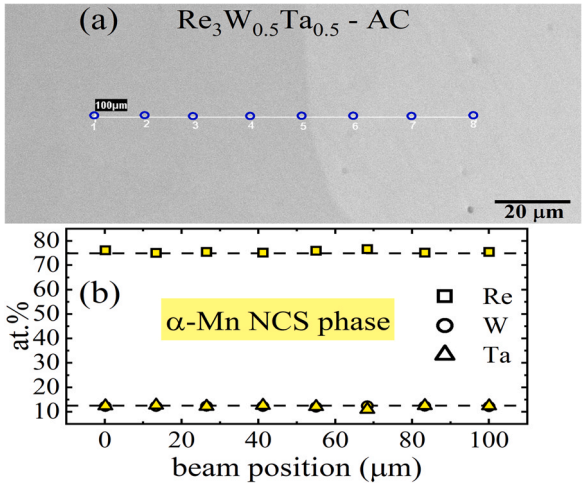

Fig. 5. (a) SEM/BSE image of the AC $Re_3W_{0.5}Ta_{0.5}$ alloy; (b) Concentration profile measured at the blue points highlighted in (a). The material displays a high degree of homogeneity in its as-cast form.

in the segregation areas. Nonetheless, the Re:W ratio of 73.7:26.3 was obtained by the WDS analysis in a 30 × 10 μm² area that includes the micro segregations, indicating that these formations do not change the overall sample composition significantly. In contrast, the concentration profile of the AC $Re_3W_{0.5}Ta_{0.5}$ solid solution (Fig. 5(b)) was found to be very uniform over 100 μm, with no significant deviation from the expected atomic ratio Ta/W/Re of 75/12.5/12.5. A similar ratio of 75/12.5/12.5 was found for the AC $Re_3W_{0.5}Nb_{0.5}$ specimens (see Supplementary material, section S4). The contrast seen in the SEM image of Fig. 5(a) is suggestive of grain with the same composition but different orientation. Therefore, as the micrograph displayed in Fig. 5(a) comes from an as-cast sample, the substitution alone is effective in promoting the phase stabilization. No distinguishable changes were noted in the micrographs of the annealed solid solutions.

We probed the superconductivity in the $Re_3W_{1-x}Nb_x$ and $Re_3W_{1-x}Ta_x$ compounds by means of measurements of field-cooled (FC) and zero-field-cooled (ZFC) dc magnetization (M). Shown in Fig. 6(a) are the M(T) data for as-cast and annealed Re_3W, as well as as-cast $Re_3W_{0.5}Nb_{0.5}$ and $Re_3W_{0.5}Ta_{0.5}$. The robust diamagnetic

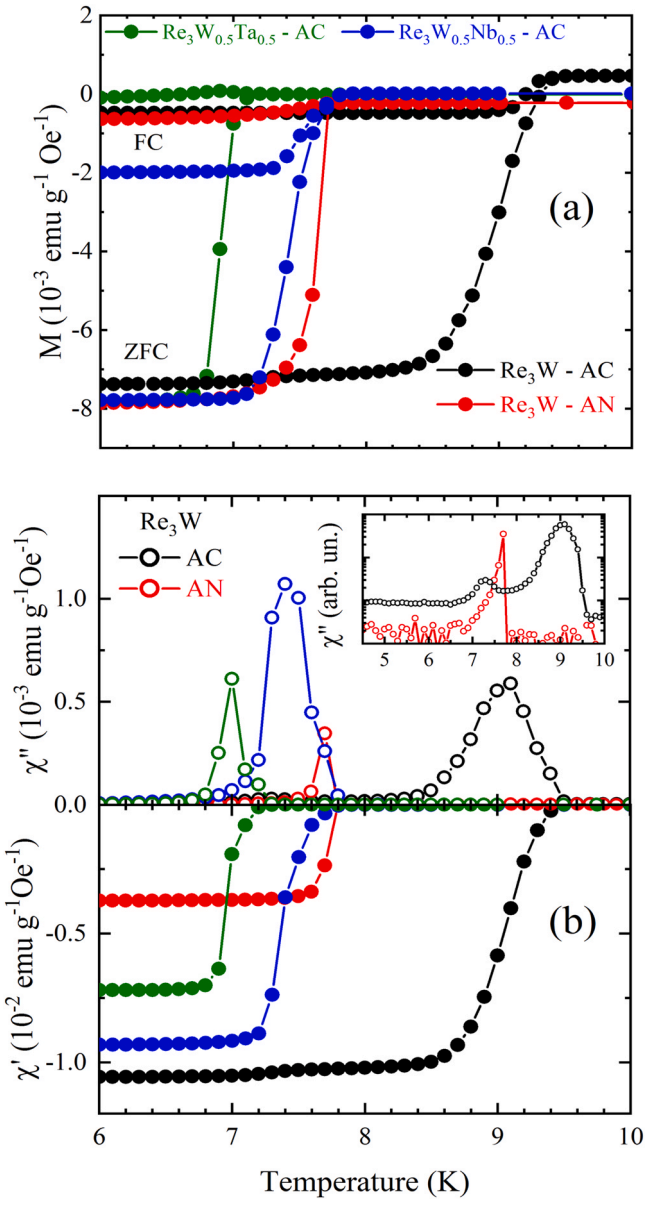

Fig. 6. Temperature dependence of (a) dc magnetization M(T) and (b) in-phase χ'(T) and out-of-phase χ''(T) *ac* magnetic susceptibility. Both measurements were conducted under H_{dc} = 5 Oe, an *ac* excitation field H_{ac} = 1 Oe, and frequency *f* = 155 Hz. Pure NCS materials (AN Re_3W, AC $Re_3W_{0.5}Ta_{0.5}$, and AC $Re_3W_{0.5}Nb_{0.5}$) display only single peaks in χ''(T). Two peaks in χ''(T) were observed in the AC Re_3W material, as seen clearly in the inset of (b).

signals below T_c in the ZFC curves are indicative of bulk superconductivity, while the weaker magnetic responses in the FC data reflect the low values of the lower critical field H_{c1} and significant flux pinning, common features of type II superconductors. The superconducting volume fractions (SVF) yielded from the ZFC M(T) data at T = 2 K are within the 150–200 % range, assuming $Re_3W_{1-x}(Ta,Nb)_x$ samples with densities in the 18.7–20.2 g cm^{-3} range. Corrections from the demagnetizing factors, as well as from more precise determinations of the remnant field of the superconducting magnet were not included in the analysis, resulting in the overestimated values of SVF.

Taking T_c from the onset of the superconducting transitions, the values of T_c for the two Re_3W specimens are ≈ 9.4 K (as-cast, multiphase) and ≈ 7.7 K (annealed, α-Mn phase). The broader transition of the AC Re_3W sample is likely due to inhomogeneities and the two-

phase character of the sample. The T_c values for the as-cast $Re_3W_{0.5}Nb_{0.5}$ and $Re_3W_{0.5}Ta_{0.5}$ are ≈ 7.6 and 7.1 K, respectively.

Low frequency (f = 155 Hz) *ac* magnetic susceptibility $\chi_{ac}(T)$ measurements near T_c are consistent with the superconducting transitions found from the dc magnetization data. The temperature dependence of the in-phase (χ'), and out-of-phase (χ'') components of χ_{ac} are shown in Figs. 6(a) and 6(b), respectively. Consistently with the dc data, $\chi'(T)$ revealed large diamagnetic shielding signals below T_c. The clear peaks in the $\chi''(T)$ data arise from the dissipation effect associated with the flux dynamics due to the onset of superconductivity.

The inset of the upper panel of Fig. 6(b) displays $\chi''(T)$ data for the AC and AN Re_3W samples. While the data for the AN sample show a single superconducting transition, the data for the AC sample show two peaks, consistently with the 2-phase character. The most prominent peak of the AC sample is centered near 9.0 K and reflects the onset of superconductivity of the majority phase, while the smaller peak in the vicinity of 7.4 K is likely due to the minority phase.

It has been reported (Refs. 27–29) that the σ and Re-h.c.p phases of the Re-W binary system are known to superconduct, and their T_c values span a rather wide temperature range from ≈ 7.4 to ≈ 9.4 K, depending on the W content (see Supplementary material, section S5). Similar behavior was observed recently in the Re-Mo system [18]. We have also observed that the $\chi''(T)$ data for the AN Re_3W sample showed just a single peak centered at ~ 7.8 K, consistent with the expected behavior of a single-phase α-Mn material [13,20]. Consistently with the expected behavior for single-phase materials, the $\chi''(T)$ data for AC $Re_3W_{0.5}Nb_{0.5}$ and $Re_3W_{0.5}Ta_{0.5}$ also revealed just a single peak at T_c, as shown in the upper panel of the Fig. 6(b).

A magnified view of the superconducting transitions is displayed in the inset of Fig. 7, showing that ρ(T) drops to zero in a very narrow temperature range for all samples. The AN Re_3W sample displays the sharpest transition, reflecting the lowest level of disorder, which can be expected given that the W sites are fully occupied only by W.

Further probing the superconducting properties of the $Re_3W_{1-x}(Nb, Ta)_x$ compounds was carried out by measurements of heat capacity. The specific heat C_p data for Re_3W (AC and AN), $Re_3W_{0.5}Nb_{0.5}$ (AC), and $Re_3W_{0.5}Ta_{0.5}$ (AC) samples near T_c are shown in Fig. 8. The C_p vs T data for the NCS single-phase AN Re_3W in Fig. 8(a) show a single jump centered in the vicinity of ~ 7.7 K, a feature consistent with the opening of a superconducting energy gap. Taking the T_c values from an entropy conservation construction, the jump

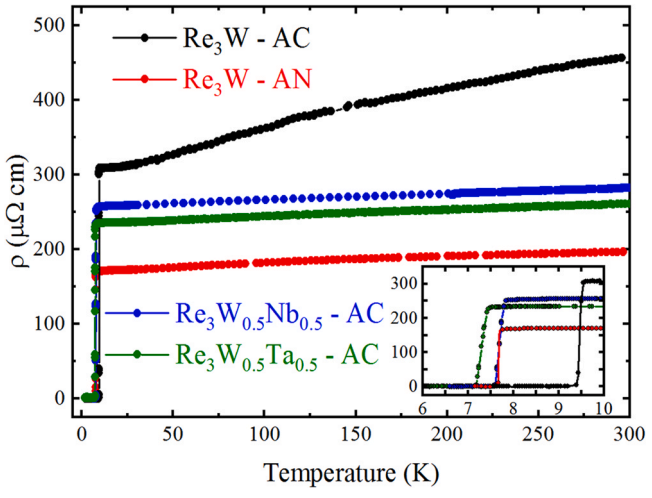

Fig. 7. Temperature dependence of the electrical resistivity ρ(T) of as-cast (AC) and annealed (AN) Re_3W and AC $Re_3W_{0.5}Ta_{0.5}$ and $Re_3W_{0.5}Nb_{0.5}$. The inset displays an expanded view of the low temperature data (T < 10 K), in order to highlight the temperature window where the superconducting transitions to the zero-resistance states are observed.

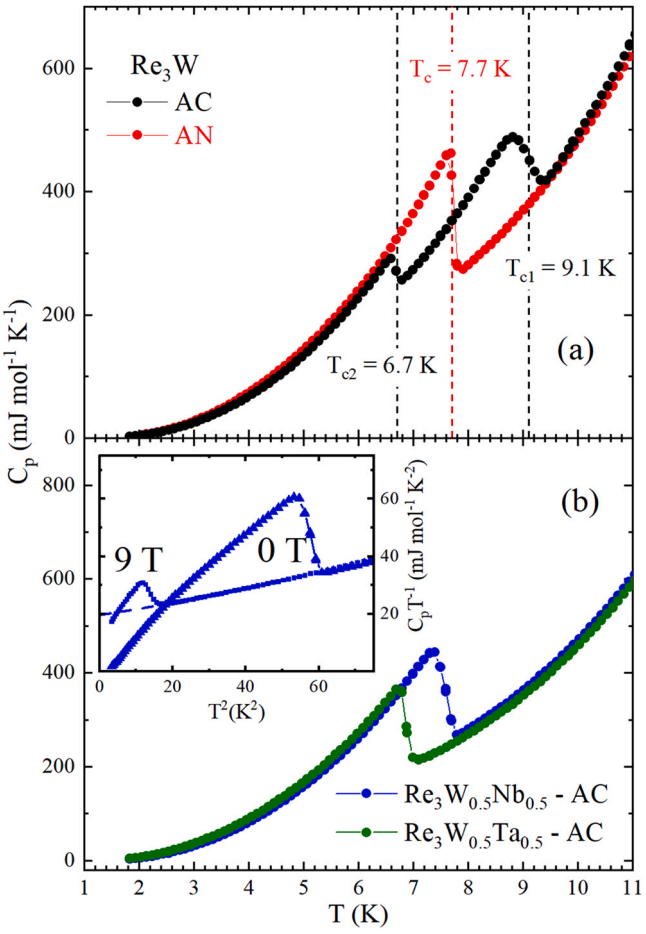

Fig. 8. (a) Temperature dependence of the specific heat of AC and AN Re_3W; and (b) AC $Re_3W_{0.5}Ta_{0.5}$ and $Re_3W_{0.5}Nb_{0.5}$. Two superconducting jumps are observed in the multi-phase AC Re_3W specimen (in black, upper panel (a)), while a single peak, in red, is observed in the AN Re_3W. The estimate of the normal state contribution to the specific heat is represented in the inset of (b).

magnitude ΔC_p is ≈ 210 mJ mol^{-1} K^{-1}, corresponds to ~ 105% of $1.43\gamma_n T_c$, the value expected from the conventional, weak-coupling BCS theory, where γ_n is the Sommerfeld electronic contribution to the specific heat (see inset of Fig. 8(b)).

The C_p vs T data for the AC Re_3W sample show two clear peaks, at T_{c1} ~ 6.7 and T_{c2} ~ 9.1 K, respectively. The higher peak centered at ~ 9.1 K corresponds to ~ 70 % (ΔC_p ~ 157 mJ mol^{-1} K^{-1}) of the BCS value, while the smaller peak near 6.7 K accounts for ~ 38 % (ΔC_p ~ 63 mJ mol^{-1} K^{-1}). Given this sizable, relatively narrow jump at T_{c2}, the superconducting phase with higher T_c makes up the major fraction of the sample volume. The two SC transitions in the $C_p(T)$ data for the AC Re_3W sample are consistent with the χ_{ac} data of Fig. 6(b). Similar $\chi_{ac}(T)$ and $C_p(T)$ behaviors were reported for as-cast Re_3W in Ref. 17; however only one feature in the $C_p(T)$ data near T ~ 9.4 K was observed in Ref. 9. The absence of a second superconducting transition in the $C_p(T)$ data from Ref. 9 suggests that the phase purity and volume fraction could depend on the details of the solidification. It is plausible that a slight difference in the cooling rate upon the solidification may yield a different fractionation of the two main AC Re_3W phases.

Shown in Fig. 8(b) are the $C_p(T)$ data for as-cast $Re_3W_{0.5}Nb_{0.5}$ and $Re_3W_{0.5}Ta_{0.5}$, displaying single jumps in $C_p(T)$ close to 7.8 and 6.9 K, respectively, consistent with the occurrence of bulk superconductivity. The C_p/T vs T^2 data for the $Re_3W_{0.5}Nb_{0.5}$ sample is shown in the inset of Fig. 8(b) in two different applied magnetic fields, H = 0 and 9 T. A linear extrapolation of the C/T vs T^2 from the

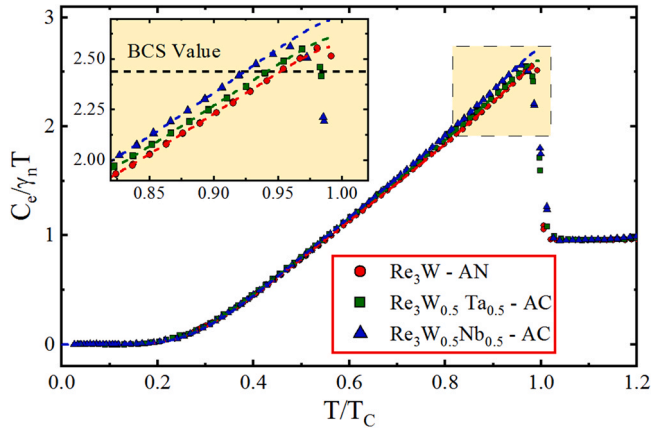

Fig. 9. The dimensionless variable $C_e(T)/\gamma_n T$ is plotted against the reduced temperature T/T_c, in order to compare the electronic contribution of the superconducting specific heat for the different specimens. Dashed red, blue, and green lines result from fitting the experimental data with the α-model. The inset shows that the superconducting jump in the vicinity of T_c for all materials slightly exceed the BCS values (black dashed line) in the weak-coupling limit.

normal phase to T = 0 yields γ_n = 17.9 mJ mol^{-1}K^{-2} for the as-cast $Re_3W_{0.5}Nb_{0.5}$ sample. In order to reduce the temperature range of the extrapolation of C_p/T vs T^2 data to T = 0 K and to obtain more reliable Sommerfeld coefficients for the Re_3W_{1-x}(Nb, Ta)$_x$ materials, the values of γ_n were taken from the $C_p(T)$ data at H = 9 T, and their values are summarized in Table 1.

The specific heat can be described by $C_p(T) = C_e(T) + C_{latt}(T)$, where $C_e(T)$ and $C_{latt}(T)$ are the electronic and phonon components, respectively. The electronic term is $C_e(T) = \gamma_n T$, and the phonon term can be written as $C_{latt}(T) = \alpha_1 T^3 + \beta_2 T^5$, where the T^3 term is the Debye low temperature approximation and the T^5 term accounts for non-harmonicities. Subtracting the fitted lattice contribution from the zero-field data allows for an estimate of the superconducting electronic contribution $C_e(T)$, which in turn permits comparing the observed behavior to the expected from the BCS theory. Displayed in Fig. 9 is a plot of $C_e(T)/\gamma_n T$ versus the reduced temperature T/T_c for the AN Re_3W and both AC $Re_3W_{0.5}Ta_{0.5}$ and $Re_3W_{0.5}Nb_{0.5}$ samples. The data for the three samples all but completely overlap, suggesting a universal behavior for this series. Therefore, the data could be fit very well to the α-model BCS [30].

The α-model BCS accounts for the strong coupling superconducting pairing, and it is based on rescaling the $\alpha = \Delta_0/k_BT$ ratio [30], an otherwise universal quantity in the BCS weak-coupling limit [31]. A model of independent fermionic excitations can be used to calculate $C_e(T)$ that is given by [32]:

$$\frac{C_e(T)}{\gamma_n T} = \frac{3\alpha^3}{\pi^2 t^3}\int_{-\infty}^{\infty} f(\varepsilon)[1 - f(\varepsilon)]\{y^2 + \delta(T)^2 - \frac{d}{dT}[\delta(T)^2]\}dy \quad (1)$$

where $f(\varepsilon)$ is the Fermi-Dirac function with $\varepsilon^2 = \Delta_0^2(y^2 + \delta(T)^2)$, $y = \xi/\Delta_0$ is the rescaled quasi-particle energy measured relative to the Fermi energy, and $\delta(T) = 1.76\ tanh(1.82[1.018(T_c/T-1)]^{0.51})$ is the temperature dependence of the gap function obtained by self-consistently solving the gap equation [33]. The α-model has been successfully applied to Re-based NCS phases [34,35], iron pnictide superconductors [36] as well as other families of superconducting materials [37].

The α values extracted from the fits yielded energy gaps of $\Delta_0 \sim$ 1.29, 1.14, and 1.28 meV for AN Re_3W, AC $Re_3W_{0.5}Ta_{0.5}$, and AC $Re_3W_{0.5}Nb_{0.5}$, respectively. These energy gaps compare well to the values of 1.25, 0.74, and 1.41 meV, respectively, reported in the literature for the parent compounds [9,10,38]. The slightly overestimate of C_e just below T_c using the strong coupling model suggests that the electron-phonon coupling in these compounds may be classified as moderate.

A dilution refrigerator was used to conduct the specific heat measurements down to T = 0.2 K, corresponding to $T/T_c \sim 0.03$ (Fig. 9), enhancing the reliability of the $C_e(T)$ analysis in the zero temperature limit. The behavior of $C_e(T)$ for the three samples is suggestive of a nodeless isotropic gap symmetry scenario, where $C_e(T)$ drops exponentially at low T/T_c. This gap symmetry has already been conjectured from the specific heat data for polycrystalline $Re_{0.82}Nb_{0.18}$ and annealed Re_3W compounds [9,21], superfluid density [20,21], and superconducting electron tunneling [38,39] measurements, although two superconducting gaps have also been suggested in the case of $Re_{0.18}Nb_{0.82}$ single crystals [40].

4. Conclusions

In summary, we synthesized Re_3W_{1-x}(Nb,Ta)$_x$ (x = 0, and 0.5) samples by arc-melting the starting materials in a water-cooled copper hearth under an UHP argon atmosphere using a tungsten electrode. The as-cast Re_3W sample was found to have two phases with two distinct superconducting transition temperatures of ~ 9.1 and 7.4 K, respectively. Single-phase, non-centrosymmetric Re_3W specimens ($T_c \sim$ 7.7 K) can only be obtained after annealing in temperatures exceeding T > 1500 °C in high vacuum. However, *as-cast specimens* with 50 % substitution of Ta or Nb for W solidify as single-phase materials with the α-Mn NCS structure, and they are more homogeneous than the annealed Re_3W specimen. Electrical resistivity, heat capacity, and magnetic susceptibility measurements indicated that the as-cast pseudo-binary alloys $Re_3W_{0.5}Ta_{0.5}$ and $Re_3W_{0.5}Ta_{0.5}$ are both superconducting, with T_c onsets of 7.1 and 7.6 K, respectively. The thermal and electrical properties suggest conventional isotropic *s*-wave superconductivity, with moderate-coupling, within the range observed in other known Re-based NCS superconducting materials. Although these materials do not reveal features of unconventional superconductivity, further studies on high-quality single crystals are in order to better probe this point. The realization that single-phase α-Mn NCS samples can be obtained directly from the melt in partially substituted $Re_3W_{0.5}Ta_{0.5}$ and $Re_3W_{0.5}Nb_{0.5}$ is of great importance for further probes of superconductivity in NCS materials.

CRediT authorship contribution statement

F. Abud: Conceptualization, Validation, Formal analysis, Investigation, Visualization, Writing – original draft, Writing – review & editing. **N. Chaia:** Investigation, Writing – original draft. **M.S. Torikachvili:** Conceptualization, Investigation, Writing – review & editing. **R.F. Jardim:** Conceptualization, Supervision, Investigation, Funding acquisition, Writing – review & editing.

Data availability

Data will be made available on request.

Declaration of Competing Interest

The authors declare that they have no known competing financial interests or personal relationships that could have appeared to influence the work reported in this paper.

Acknowledgments

The authors gratefully acknowledge the fruitful discussions with Gilberto A. Coelho, Antonio J. S. Machado, Lucas E. Correa, and Rodolfo da Silva Teixeira. This research was partially supported by

the Technological Characterization Laboratory from USP (LCT-USP). This material is based upon research supported by Brazil's agencies FAPESP (Grants No. 2013/07296–2, 2019/26141–6, 2022/02691–0, and 2022/10874–7), CNPq (Grant No. 301463/2019–0), and CAPES (Finance Code 001).

Appendix A. Supporting information

Supplementary data associated with this article can be found in the online version at doi:10.1016/j.jallcom.2023.170259.

References

[1] L.P. Gor'kov, E.I. Rashba, Superconducting 2D system with lifted spin degeneracy: mixed singlet-triplet state, Phys. Rev. Lett. 87 (2001) 037004.
[2] M. Smidman, M.B. Salamon, H.Q. Yuan, D.F. Agterberg, Superconductivity and spin-orbit coupling in non-centrosymmetric materials: a review, Rep. Prog. Phys. 80 (2017) 46.
[3] P.W. Anderson, Structure of "triplet" superconducting energy gaps, Phys. Rev. B 30 (1984) 4000.
[4] D. Singh, J.A.T. Barker, A. Thamizhavel, D. McK. Paul, A.D. Hillier, R.P. Singh, Time-reversal symmetry breaking in the noncentrosymmetric superconductor Re_6Hf: further evidence for unconventional behavior in the α-Mn family of materials, Phys. Rev. B 96 (2017) 180501.
[5] R.P. Singh, A.D. Hillier, B. Mazidian, J. Quintanilla, J.F. Annett, D.M. Paul, G. Balakrishnan, M.R. Lees, Detection of time-reversal symmetry breaking in the noncentrosymmetric superconductor Re_6Zr using muon-spin spectroscopy, Phys. Rev. Lett. 112 (2014) 107002.
[6] D. Singh, K.P. Sajilesh, J.A.T. Barker, D. McK. Paul, A.D. Hillier, R.P. Singh, Time-reversal symmetry breaking in the noncentrosymmetric superconductor Re_6Ti, Phys. Rev. B 97 (2018) 100505.
[7] T. Shang, et al., Nodeless superconductivity and time-reversal symmetry breaking in the noncentrosymmetric superconductor $Re_{24}Ti_5$, Phys. Rev. B 97 (2018) 020502.
[8] T. Shang, et al., Time-reversal symmetry breaking in Re-based superconductors, Phys. Rev. Lett. 121 (2018) 257002.
[9] P.K. Biswas, A.D. Hillier, M.R. Lees, D.M. Paul, Comparative study of the centrosymmetric and noncentrosymmetric superconducting phases of Re_3W using muon spin spectroscopy and heat capacity measurements, Phys. Rev. B 85 (2012) 134505.
[10] J.A.T. Barker, B.D. Breen, R. Hanson, A.D. Hillier, M.R. Lees, G. Balakrishnan, D. McK. Paul, R.P. Singh, Superconducting and normal-state properties of the noncentrosymmetric superconductor Re_3Ta, Phys. Rev. B 98 (2018) 104506.
[11] Arushi, D. Singh, P.K. Biswas, A.D. Hillier, R.P. Singh, Unconventional superconducting properties of noncentrosymmetric $Re_{5.5}Ta$, Phys. Rev. B 101 (2020) 144508.
[12] Z.-K. Liu, Y.A. Chang, Evaluation of the thermodynamic properties of the Re–Ta and Re–W systems, J. Alloy. Compd. 299 (2000) 153.
[13] P.K. Biswas, M.R. Lees, A.D. Hillier, R.I. Smith, W.G. Marshall, D.M. Paul, Structure and superconductivity of two different phases of Re_3W, Phys. Rev. B 84 (2011) 184529.
[14] S.H. Zhou, Z.-K. Liu, Evaluation of the thermodynamic properties and phase equilibria of the Re-Ta-W system, Metall. Mater. Trans. A 33 (2002) 2781.
[15] F.J. Spooner, C.G. Wilson, Ordering in binary σ phases, Acta Crystallogr 17 (1964) 12.
[16] J.-M. Joubert, J.-C. Crivello, Non-stoichiometry and calphad modeling of Frank-Kasper phases, Appl. Sci. 2 (2012) 3.
[17] Y. Jing, S. Lei, L. Qiang, W. Wei-Hua, W. Hai-Hu, Specific heat of the non-centrosymmetric superconductor Re3W, Chin. Phys. B 18 (2009) 704.
[18] T. Shang, D.J. Gawryluk, J.A.T. Verezhak, E. Pomjakushina, M. Shi, M. Medarde, J. Mesot, T. Shiroka, Structure and superconductivity in the binary $Re_{1-x}Mo_x$ alloys, Phys. Rev. Mater. 3 (2019) 024801.
[19] J. Rodríguez-Carvajal, Recent advances in magnetic-structure determination by neutron powder diffraction, Phys. B 192 (1993) 55.
[20] Y.L. Zuev, V.A. Kuznetsova, R. Prozorov, M.D. Vannette, M.V. Lobanov, D.K. Christen, J.R. Thompson, Evidence for S-wave superconductivity in non-centrosymmetric Re_3W from magnetic penetration depth measurements, Phys. Rev. B 76 (2007) 132508.
[21] J. Chen, L. Jiao, J.L. Zhang, Y. Chen, L. Yang, M. Nicklas, F. Steglich, H.Q. Yuan, BCS-like superconductivity in the noncentrosymmetric compounds Nb_xRe_{1-x} ($0.13 \le x \le 0.38$), Phys. Rev. B 88 (2013) 144510.
[22] R. Steadman, P.M. Nuttall, χ phase in a niobium-rhenium alloy, Acta Cryst. 1 (1964) 62–63.
[23] H. Okamoto, Re-Ta (Rhenium-Tantalum), Binary Alloy Phase Diagrams, ASM International, Materials Park, Ohio, 1990, pp. 3207–3208.
[24] H. Okamoto, Re-W (Rhenium-Tungsten), Binary Alloy Phase Diagrams, ASM International, Materials Park, Ohio, 1990, pp. 3218–3219.
[25] I.A. Tregubov, L.N. Evseyeva, O.S. Ivanov, I.D. Marchuko, Investigation of W-Ta-Re constitution diagram by diffusion layer method, Russ. Metall. 1 (1973) 144.
[26] J.-M. Joubert, M. Phejar, Crystal chemistry and calphad modelling of the χ phase, Prog. Mater. Sci. 54 (2009) 945.
[27] C.W. Chu, W.L. McMillan, H.L. Luo, Superconductivity of Re-Os, Re-Ru, Ru-Os, and Re-W HCP alloys systems and slightly doped Re, Phys. Rev. B 3 (1971) 3757.
[28] J.K. Hulm, R.D. Blaugher, Superconducting solid solution alloys of transition elements, Phys. Rev. 123 (1961) 1569.
[29] R.D. Blaugher, J.K. Hulm, Superconductivity in the σ and α-Mn structures, J. Phys. Chem. Solids 19 (1961) 134.
[30] H. Padamsee, J.E. Neighbor, C.A. Shiffman, Quasiparticle phenomenology for thermodynamics of strong-coupling superconductors, J. Low. Temp. Phys. 12 (1973) 387.
[31] J. Bardeen, L.N. Cooper, J.R. Schrieffer, Theory of superconductivity, Phys. Rev. 108 (1957) 1175.
[32] J.B. Ketterson, S.N. Song, Calculation of the thermodynamic properties using the Bogoliubov-Valatin Method, Superconductivity, first ed., Cambridge University Press, Cambridge; New York, 1999, pp. 212–215.
[33] A. Carrington, F. Manzano, Magnetic penetration depth of MgB_2, Phys. C. -Supercond.Appl. 385 (2003) 205.
[34] D. Singh, A.D. Hillier, A. Thamizhavel, R.P. Singh, Superconducting properties of the noncentrosymmetric superconductor Re_6Hf, Phys. Rev. B 94 (2016) 054515.
[35] D.A. Mayoh, J.A.T. Barker, R.P. Singh, G. Balakrishnan, D. McK. Paul, M.R. Lees, Superconducting and normal-state properties of the noncentrosymmetric superconductor Re_6Zr, Phys. Rev. B 96 (2017) 064521.
[36] P. Popovich, A.V. Boris, O.V. Dolgov, A.A. Golubov, D.L. Sun, C.T. Lin, R.K. Kremer, B. Keimer, Specific heat measurements of $Ba_{0.68}K_{0.32}Fe_2As_2$ single crystals: evidence for a multiband strong-coupling superconducting state, Phys. Rev. Lett. 105 (2010) 027003.
[37] F. Abud, L.E. Correa, I.R. Souza Filho, A.J.S. Machado, M.S. Torikachvili, R.F. Jardim, Absence of superconductivity in NbB, Phys. Rev. Mater. 1 (2017) 044803.
[38] C. Cirillo, G. Carapella, M. Salvato, R. Arpaia, M. Caputo, C. Attanasio, Superconducting properties of noncentrosymmetric $Nb_{0.18}Re_{0.82}$ thin films probed by transport and tunneling experiments, Phys. Rev. B 94 (2016) 104512.
[39] Y. Huang, J. Yan, Y.L. Wang, L. Shan, Q. Luo, W. Wang, H.H. Wen, Isotropic S-wave pairing symmetry in non-centrosymmetric Re_3W revealed by point-contact spectroscopy, Supercond. Sci. Technol. 21 (2008) 075011.
[40] C. Cirillo, R. Fittipaldi, M. Smidman, G. Carapella, C. Attanasio, A. Vecchione, R.P. Singh, M.R. Lees, G. Balakrishnan, M. Cuoco, Evidence of double-gap superconductivity in noncentrosymmetric $Nb_{0.18}Re_{0.82}$ single crystals, Phys. Rev. B 91 (2015) 134508.